Controlling the Spectral Characteristics of a Spin-Current Auto-Oscillator with an Electric Field

R. H. Liu (刘荣华),[1,2,*] Lina Chen,[1] S. Urazhdin,[2] and Y. W. Du (都有为)[1]

[1]*National Laboratory of Solid State Microstructures, School of Physics and Collaborative Innovation Center of Advanced Microstructures, Nanjing University, Nanjing 210093, China*

[2]*Department of Physics, Emory University, Atlanta, Georgia 30322, USA*

(Received 11 March 2017; revised manuscript received 8 June 2017; published 9 August 2017)

We study the effects of electrostatic gating on the magnetization auto-oscillations induced by the local injection of electric current into a ferromagnet–heavy-metal bilayer. We find that the characteristic currents required for the excitation, the intensity, and the spectral characteristics of the generated dynamical states can be tuned by the voltage applied to the metallic gate separated from the bilayer by a thin insulating layer. We show that the effect of electrostatic gating becomes enhanced in the strongly nonlinear oscillation regime at sufficiently large driving currents. Analysis shows that the observed effects are caused by a combination of electric-field-dependent surface anisotropy and electric-field-dependent contribution to the current-induced spin-orbit torques. The demonstrated ability to control the microwave emission and spectral characteristics provides an efficient approach to the development of electrically tunable microwave nano-oscillators.

DOI: 10.1103/PhysRevApplied.8.021001

Significant progress has been made in recent years in the ability to control magnetism by magnetic field, current-induced spin torques, electrostatic gating, and optical fields. All-electronic control of magnetization, achieved by the application of electric fields [1], electric currents [2], or a combination of both, is particularly attractive, because it provides the benefits of high speed, low power, the possibility of downscaling for high-density applications, and is amenable to integration with the modern semiconductor electronics. Several approaches and mechanisms enabling all-electric control of magnetism have been extensively investigated in a number of materials and heterostructure geometries. For instance, the Curie temperature has been varied in magnetic semiconductors by the modulation of the carrier concentration [3,4]. Electrically driven magnetization reversal has been achieved in multiferroic materials due to its coupling to the electric polarization [5–7] and in ultrathin ferromagnet-oxide heterostructures due to the voltage dependence of the interfacial magnetic anisotropy [8–10]. Magnetization control by current, including current-induced magnetization reversal and auto-oscillations due to the spin transfer torque (STT), has been achieved in magnetic multilayer structures [11–14] and in heavy-metal–ferromagnet heterostructures (FH) [15–18]. In FH bilayers, STT is produced by the pure spin current generated by a combination of the spin Hall effect (SHE) inside the heavy metal and the Rashba effect caused by the spin-orbit interaction at the magnetic interface [19–23]. The recently demonstrated electric-field-assisted current-induced magnetization reversal in magnetic tunnel junctions has received significant attention due to the flexibility of control and the high efficiency of the combined electric-field effect and current-induced spin torques [24,25]. Despite these promising features, the mechanisms of the electric-field effect on the current-induced spin torques and magnetization dynamics are still being debated.

Here, we demonstrate the effects of the electric field on the magnetization oscillation driven by the current-induced spin-orbit torques in a spin-current auto-oscillator (SCAO) based on the permalloy-platinum (Py/Pt) bilayer. The highly coherent self-localized spin wave is excited in the extended Py film by the local injection of spin current. We show that the electric field produced by the backgating can modify the characteristic currents required for the auto-oscillation, as well as the spectral characteristics of the auto-oscillation, due to a combination of field-induced spin-orbit torques and the modulation of interfacial magnetic anisotropy. We also demonstrate that the effects of the electric field can be significantly enhanced in the strongly nonlinear dynamical regime of SCAO achieved at sufficiently large driving currents.

Figure 1(a) shows the schematic of the test device structure and the experimental setup. The device is fabricated on an annealed sapphire substrate by a combination of magnetron sputtering and *e*-beam lithography. The SCAO is based on a Py(3)/Pt(2) FH bilayer disk with a 4-μm diameter. All thicknesses are given in nanometers. Two Au(100) electrodes with sharp tips separated by an 80-nm gap, fabricated on top of the FH bilayer, are utilized to locally inject the electrical current into the bilayer. The spin Hall effect, generated by the current flowing through Pt due to the spin-orbit interaction, produces a pure spin current

*rhliu@nju.edu.cn

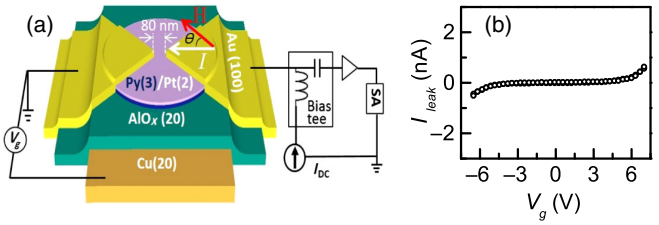

FIG. 1. (a) Schematic of the device structure and the experimental setup. (b) Gate leakage current I_{leak} vs gate voltage V_g for a gated SCAO device.

flowing into the Py(3) layer, exerting STT on its magnetization. An additional torque is exerted on the Py magnetization due to the Rashba spin-orbit interaction at the Py/Pt and Py/AlO_x interfaces. This structure and its operation are similar to the planar point contact spin Hall nano-oscillators previously studied by optical [18] and magnetoelectronic techniques [26]. In our study, the device includes an additional Cu(20) gate electrode fabricated underneath the FH bilayer, and electrically isolated from it by an $AlO_x(20)$ layer. Figure 1(b) shows the dependence of the leakage current I_{leak} between the FH and the gate electrode on the voltage V_g applied to the gate. The leakage does not exceed 100 pA at gate voltages of up to ± 5 V, indicating a high quality of the AlO_x insulator characterized by the breakdown electric field of more than 4 MV/cm. All the measurements described below are performed at temperature $T = 6$ K, and a fixed angle $\theta = 30°$ between the in-plane field and the direction of current driving the SCAO.

Spectroscopic measurements of the microwave generation and the spin-torque-induced ferromagnetic resonance (ST-FMR) performed at zero gate voltage allow us to characterize the magnetic properties and the spectral characteristics of the SCAO (Fig. 2). Auto-oscillations, indicated by the abrupt emergence of a sharp spectral peak, are observed above the critical current $I_c \approx 5.7$–6.1 mA in the studied range of fields. The value of I_c is significantly smaller than in the previously studied planar point contact spin Hall oscillators based on thicker Py/Pt bilayers [18,26], due to a combination of the more efficient spin injection from the thin Pt layer [27] and the larger effects of spin current on the relatively thin Py layer.

Figure 2(a) shows an example of the auto-oscillation spectra acquired at $I = 6.7$ mA, and the applied field ranging from 200 to 750 Oe. The spectral peak is well approximated by the Lorentzian function, as shown by the solid curves. Spectral characteristics such as the full width at half maximum (FWHM), the central peak frequency f_0, and the generated power P are extracted from the Lorentzian fitting. Figures 2(b) and 2(c) show the dependence of the minimum linewidth and the maximum integral intensity on field, both of which are observed at currents close to the same value I_p corresponding to the largest amplitude of the microwave generation peak. The auto-oscillation frequency also exhibits a maximum at the same

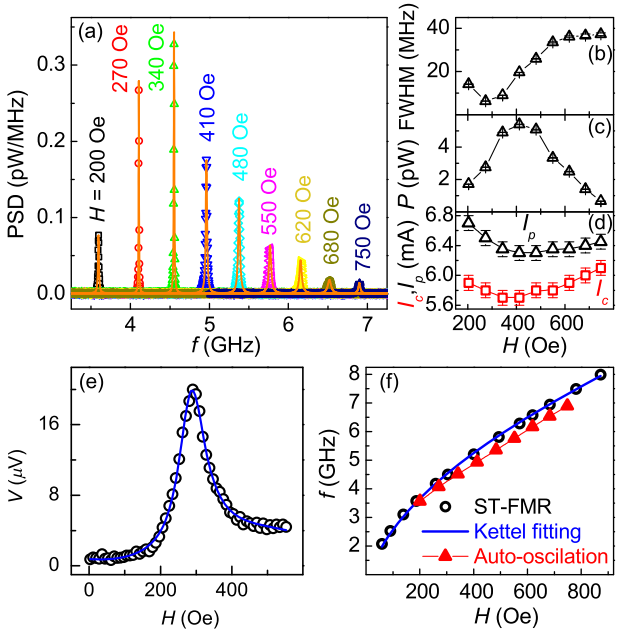

FIG. 2. Dependence of the microwave generation characteristics on the magnetic field H, at $V_g = 0$. (a) Generation spectra (symbols) obtained at $I = 6.7$ mA and the labeled values of the magnetic field. The curves are the results of fitting by the Lorentzian function. (b)–(d) Field dependencies of the minimum full width at half-maximum of the generation spectrum (b), the maximum integral intensity (c), and the currents I_c (squares) and I_p (triangles) defined in the text (d). (e) Magnetic field dependence of the ST-FMR voltage obtained with a microwave current of $I_{\text{ac}} = 1$ mA rms at frequency $f_{\text{ext}} = 4$ GHz. The curve is the best fit with a sum of a symmetric and an antisymmetric Lorentzian. (f) The ST-FMR frequency (circles) and the maximum frequency of the auto-oscillation (triangles) vs H. The solid curve is the result of fitting with the Kittel formula $f = \gamma\sqrt{H(H + H_d)}$, where $\gamma = 2.8$ MHz/Oe is the gyromagnetic ratio, and the effective demagnetizing field H_d has the best-fit value of 8.4 kOe determined by the magnetization of permalloy (Py) and the surface anisotropy.

current value I_p. The linewidth is small at low fields, with a minimum of 6 MHz at $H = 270$ Oe, and gradually increases at larger fields to 36 MHz at $H = 750$ Oe [Fig. 2(b)]. The integral intensity P exhibits a nonmonotonic dependence on the field, with a broad maximum near the field $H \approx 400$ Oe somewhat larger than that corresponding to the minimum linewidth. Both I_p and the critical current I_c for the onset of auto-oscillation exhibit a broad minimum of 6.3 and 5.7 mA, respectively, around the same field $H \approx 400$ Oe [Fig. 2(d)]. The observed variations of auto-oscillation characteristics are likely associated with the field dependence of the dynamical mode spectrum in the point contact region of the Py(3) film. In particular, the increase of the minimum linewidth and of the critical current, and the decrease of the maximum generated power at large fields, are indicative of the presence of a secondary dynamical mode whose frequency is close to the oscillation

frequency [26,28], resulting in a reduced coherence and amplitude of auto-oscillation [29–31].

The magnetic properties of the Py film and the nature of the auto-oscillation mode are established by the ST-FMR technique [32]. A microwave current with an rms amplitude of 1 mA is applied to SCAO, resulting in the magnetization oscillation at the same frequency. The oscillation amplitude is characterized by the dc voltage produced due to mixing of the resistance oscillation with the ac current. The dependence of the dc voltage on the field could be well fitted by a sum of a symmetric and an antisymmetric Lorentzian, as illustrated in Fig. 2(e) for a typical ST-FMR curve. Figure 2(f) shows the field dependence of the FMR frequency f_{FMR} and of the maximum auto-oscillation frequency f_0 reached at $I = I_p$. These data show that the auto-oscillation frequency always remains lower than f_{FMR}, consistent with the properties of other in-plane magnetized SCAO [18,26]. These behaviors can be attributed to the nonlinear nature of the auto-oscillation mode, which forms a self-localized standing spin-wave "bullet" [29]. We note that the frequency of auto-oscillation approaches f_{FMR} at small $H \sim 200$ Oe. This explains the low-field broadening of the auto-oscillation spectrum [Fig. 2(b)], since a larger spectral overlap between the auto-oscillation and the linear spin wave spectrum results in larger radiation losses. The ST-FMR data can be fitted with the Kittel formula

$$f = \gamma\sqrt{H(H + H_d)}, \tag{1}$$

where γ is the gyromagnetic ratio, and H_d is the effective demagnetizing field. We note that spin-orbit coupling at Py/Pt and Py/AlO_x interfaces results in uniaxial magnetic anisotropy of the ultrathin Py(3) layer, with the anisotropy axis normal to the film. This contribution can be taken into account as an additional term in the effective demagnetizing field $H_d = 4\pi M - (2K/tM)$, where K is the anisotropy coefficient, and $t = 3$ nm is the thickness of the Py film. The magnitude $K = 0.27$ erg/cm^2 of the interfacial magnetic anisotropy is obtained from fitting the ST-FMR data using the saturation magnetization $M_s = 840$ emu/cm^3 previously determined for similar Py films [26].

Our central experimental result is the dependence of the magnetization oscillation characteristics on the electric field produced by the gate voltage V_g. We analyze this effect at field $H = 340$ Oe, at which the SCAO produces a large generation power and a narrow spectral linewidth [Figs. 2(b) and 2(c)]. Figures 3(a) and 3(b) show the power spectral density of the oscillation spectra at $I = 6.2$ and 6.7 mA, respectively, for the bias voltage V_g ranging from -5 to $+5$ V. The shift $\Delta f(V_g) = f_0(V_g) - f_0(0)$ of the central oscillation frequency exhibits a linear dependence on V_g with the slope of 4.6 MHz/V at $I = 6.2$ mA, as shown in the inset of Fig. 3(a). In addition to this shift, at

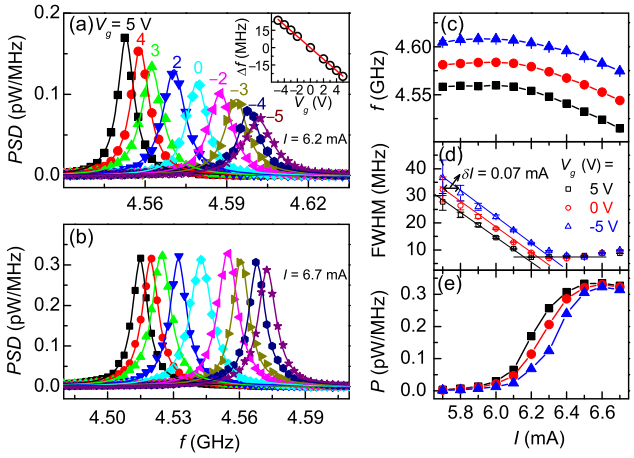

FIG. 3. Effects of electrostatic gating on the microwave generation characteristics of SCAO. (a) Symbols: Power spectral density (PSD) of generation spectra at the labeled values of the gate voltage V_g ranging from -5 to 5 V, at $H = 340$ Oe and $I = 6.2$ mA. The curves are the results of fitting by the Lorentzian function. Inset: dependence of the central frequency shift $\Delta f(V_g) = f_0(V_g) - f_0(0)$ of the spectral peak on the gate voltage (symbols), and the linear fit of the data (line). (b) Same as (a), at $I = 6.7$ mA. (c)–(e) Dependence of the central generation frequency f_0 (c), the linewidth FWHM (d), and the integral intensity P (e) on current I at $V_g = -5$ (triangles), 0 (circles), and 5 V (squares). The central frequency and the linewidth are determined by fitting the power spectra with the Lorentzian function, as shown in (a) and (b). The solid lines in (d) are the linear fits that are used to determine the effective excitation current shift $\delta I(\pm 5\ \mathrm{V}) = \pm 0.07$ mA.

$I = 6.2$ mA the intensity of the spectral peak also varies with the gate voltage. Meanwhile, at $I = 6.7$ mA, gating produces only a frequency shift at a rate of 6 MHz/V. The difference between the effects of gating at these two currents is closely correlated with the current dependence of the oscillation characteristics, as discussed below.

Figures 3(c)–3(e) show the current dependencies of the central oscillation frequency, the linewidth, and the generation power, measured at $V_g = -5$, 0, and 5 V. The frequency and the generation power slowly increase, and the linewidth linearly decreases at small currents. At currents above 6.1 mA, the generated power rapidly increases, the frequency exhibits a strong redshift, while the linewidth remains approximately constant. Similarly, behaviors have been observed both in the spin valve nano-oscillators [33] and in spin Hall oscillators [26], and are consistent with the nonlinear theory of magnetic nano-oscillators [31]. We note that the crossover at $I = 6.1$ mA superficially resembles a transition from the regime of spin-current-enhanced thermal fluctuations at smaller currents to auto-oscillation at larger current. However, the oscillation frequency is below f_{FMR} even at small currents, and therefore this dynamical state does not belong to the linear spin-wave spectrum and cannot be attributed to thermal fluctuations.

As is apparent from Fig. 3(c), the effect of gating on the oscillation frequency can be described as being mostly a vertical shift. This observation is consistent with the previous studies of the effects of gating in thin magnetic films, which demonstrated the possibility to modify the coercive field [8] and even switch the magnetization direction [10]. These effects could be attributed to the modulation of the surface magnetic anisotropy, mostly due to the variation of the Fermi level at the interfaces [34]. In our measurements, the frequency of the oscillation also depends on the interfacial magnetic anisotropy, described as a contribution to the effective demagnetizing field H_d in the Kittel formula Eq. (1). Based on the data of Fig. 3(c) at currents below 6.1 mA and the Kittel formula, we estimate that the electrostatic gating modulates the interfacial anisotropy coefficient at the rate of $dK/dV_g = 2.2 \times 10^{-3}$ erg/(V cm^2).

Anisotropy modulation is expected to provide a contribution that is independent of the oscillation regime of SCAO. However, the observed effects of gating depend on the nonlinear regime of oscillation. At currents below the nonlinear crossover, the oscillation linewidth is modified by the electric field [Fig. 3(d)], while it is not significantly affected by gating at currents above the crossover. This effect can be approximately described as an effective current shift of $\delta I(V_g) = \pm 0.07$ mA for $V_g = \pm 5$ V. The effect of gating on the current-dependent generation power can be similarly described as an effective shift of the driving current [Fig. 3(e)]. If the observed effective current shift of 70 μA at $V_g = \pm 5$ V were caused by the modulation of interfacial anisotropy, the rate of anisotropy modulation would be $dK/dV_g \sim 35 \times 10^{-3}$ erg/(V cm^2), as estimated from the dependence of I_c and I_p on H in Fig. 2(d). This value is 15 times larger than estimated from the frequency shift in Fig. 3(e), indicating that anisotropy variation alone cannot explain the observed effects.

The observed effective current shift indicates that the dampinglike current-induced torque is modulated by gating. This torque comprises two different contributions: one from the bulk SHE in Pt, another from the Rashba-like contribution from the Py/AlO$_x$ and Py/Pt interfaces. Since the electric field is efficiently screened in the metallic Py(3) layer, we conclude that only the Rashba contribution from the Py/AlO$_x$ interface contributes to the observed modulation. An additional Rashba-type fieldlike torque that acts as an effective field H_{ST} and can modulated the frequency. At current density $j \sim 10^8$ A/cm^2, we estimate Rashab-like $H_{ST} < 50$ Oe [23,35,36], less than ~2% of the interfacial anisotropy field H_k, providing a negligible contribution to the oscillation frequency. Unlike fieldlike torque, dampinglike torque counteracts Gilbert damping, contributing to the dependence of magnetization precession on current. The voltage-dependent Rashba dampinglike torque $\Gamma_\parallel$ is expected to result in an effective rescaling of the driving current, which for a small current range is approximately equivalent to a current shift δI. The 1.1% variation of $\Gamma_\parallel$ at $V_g = 5$ V obtained in our measurements is comparable to that reported for Pt/Co/AlO$_x$ [35].

The data of Fig. 3 clearly demonstrate two different effects of gating, one resulting from the field-dependent surface anisotropy, another from the Rashba-like $\Gamma_\parallel$. To quantitatively analyze their respective contributions to the oscillation frequency, we can write

$$df/dV_g = \frac{\partial f(I,K)}{\partial K}\frac{dK}{dV_g} + \frac{\partial f(I,K)}{\partial I}\frac{dI}{dV_g}, \qquad (2)$$

where the first term represents the contribution of the surface anisotropy, and the second term comes from the spin-orbit torque. The second contribution is determined by the frequency nonlinearity of the oscillator described by $\partial f(I,K)/\partial I$. The voltage dependence of the interfacial anisotropy is not directly affected by the nonlinearity, and is expected to be approximately independent of the driving current.

The presented analysis demonstrates that the frequency nonlinearity of the oscillator can provide a significant contribution to the gating effects. In the studied SCAO, the magnitude of the nonlinearity remains small at currents up to $I = 6.2$ mA, and exhibits a significant increase at larger currents, as illustrated by the current dependence of f and df/dI at $V_g = 0$ in Fig. 4(a). Since the frequency nonlinearity is weak at $I < 6.1$ mA, the contribution of the effective current shift to the frequency shift is small. As a consequence, the gating effect is dominated by the variation of the surface anisotropy, independent of current. Indeed, the magnitude of the frequency shift $|\Delta f| \approx 24$ MHz at $V_g = \pm 5$ V remains approximately constant in this current range [Fig. 4(b)]. At $I > 6.1$ mA, the nonlinearity plays an increasingly significant role, as reflected by the increasing frequency shift in Fig. 4(b). We can estimate the value of

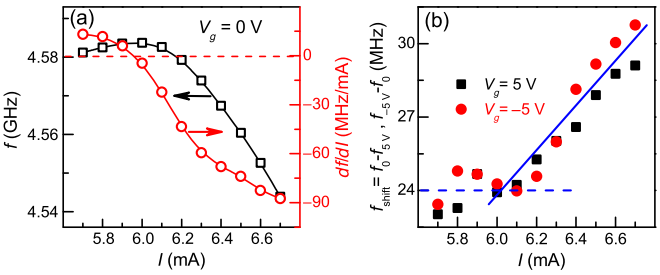

FIG. 4. Analysis of the current dependence of the electric-field effects. (a) Center frequency of the auto-oscillation (left vertical axis) and its differential df/dI (right vertical axis) vs I, at $V_g = 0$ and $H = 340$ Oe. (b) The current dependence of the frequency shifts $f(0) - f(5\text{ V})$ (squares) and $f(-5\text{ V}) - f(0)$ (circles), with the respective currents offset by $\Delta I(5\text{ V}) = 0.07$ mA for $V_g = 5$ V and $\Delta I(-5\text{ V}) = -0.07$ mA for $V_g = -5$ V. The dashed line indicates the current-independent frequency shift at $I < 6.1$ mA. The solid line is a linear fit for the $I > 6.1$ mA data.

$dI/dV_g \approx -0.014$ mA/V in the second term in Eq. (2) from the dependencies of the linewidth and the generation power on the gate voltage [Figs. 3(d) and 3(e)]. Based on the value of $\partial f/\partial I = -85$ MHz/mA at $I = 6.7$ mA determined from Fig. 4(a), we calculate the contribution $|\Delta f_I| = 6.0$ MHz to the overall frequency shift at this current and $V_g = \pm 5$ V. This result is consistent with the total observed shift of 30 MHz.

In summary, we demonstrate that dynamical magnetization states excited by spin current in magnetic nano-oscillators based on spin-orbit torques can be controlled by electrostatic gating. The observed effects are produced by two distinct contributions, one caused by the field-dependent interfacial magnetic anisotropy, another by the modulation of the Rashba-like interfacial dampinglike torque. The former results mostly in the oscillation frequency shift, while the latter is approximately equivalent to a shift of the driving current. Our results also indicate that this mechanism can be particularly effective in strongly nonlinear oscillators. Electric-field modulation of the current-induced magnetization oscillations and spin waves can be utilized for frequency mixing, synchronization, and in logic gates in spin wave-based electronic (magnonic) devices.

ACKNOWLEDGMENTS

R. H. L., L. N. C., and Y. W. D. are supported by the National Key Research and Development Program of China (Grant No. 2016YFA0300803), the Open Research Fund of Jiangsu Provincial Key Laboratory for Nanotechnology, and the Fundamental Research Funds for the Central Universities. S. U. acknowledges support from NSF Grants No. ECCS-1503878 and No. DMR-1504449.

[1] F. Matsukura, Y. Tokura, and H. Ohno, Control of magnetism by electric fields, Nat. Nanotechnol. **10**, 209 (2015).
[2] A. Brataas, A. D. Kent, and H. Ohno, Current-induced torques in magnetic materials, Nat. Mater. **11**, 372 (2012).
[3] H. Ohno, D. Chiba, F. Matsukura, T. Omiya, E. Abe, T. Dietl, Y. Ohno, and K. Ohtani, Electric-field control of ferromagnetism, Nature (London) **408**, 944 (2000).
[4] D. Chiba, M. Yamanouchi, F. Matsukura, and H. Ohno, Electrical manipulation of magnetization reversal in a ferromagnetic semiconductor, Science **301**, 943 (2003).
[5] D. Lebeugle, A. Mougin, M. Viret, D. Colson, and L. Ranno, Electric Field Switching of the Magnetic Anisotropy of a Ferromagnetic Layer Exchange Coupled to the Multiferroic Compound $BiFeO_3$, Phys. Rev. Lett. **103**, 257601 (2009).
[6] J. T. Heron, M. Trassin, K. Ashraf, M. Gajek, Q. He, S. Y. Yang, D. E. Nikonov, Y. H. Chu, S. Salahuddin, and R. Ramesh, Electric-Field-Induced Magnetization Reversal in a Ferromagnet-Multiferroic Heterostructure, Phys. Rev. Lett. **107**, 217202 (2011).
[7] Y. Tokunaga, Y. Taguchi, T.-h. Arima, and Y. Tokura, Electric-field-induced generation and reversal of ferromagnetic moment in ferrites, Nat. Phys. **8**, 838 (2012).
[8] M. Weisheit, S. Faehler, A. Marty, Y. Souche, C. Poinsignon, and D. Givord, Electric field-induced modification of magnetism in thin-film ferromagnets, Science **315**, 349 (2007).
[9] T. Maruyama, Y. Shiota, T. Nozaki, K. Ohta, N. Toda, M. Mizuguchi, A. A. Tulapurkar, T. Shinjo, M. Shiraishi, S. Mizukami, Y. Ando, and Y. Suzuki, Large voltage-induced magnetic anisotropy change in a few atomic layers of iron, Nat. Nanotechnol. **4**, 158 (2009).
[10] Y. Shiota, T. Nozaki, F. Bonell, S. Murakami, T. Shinjo, and Y. Suzuki, Induction of coherent magnetization switching in a few atomic layers of FeCo using voltage pulses, Nat. Mater. **11**, 39 (2012).
[11] J. C. Slonczewski, Current-driven excitation of magnetic multilayers, J. Magn. Magn. Mater. **159**, L1 (1996); Excitation of spin waves by an electric current, J. Magn. Magn. Mater. **195**, L261 (1999).
[12] L. Berger, Emission of spin waves by a magnetic multilayer traversed by a current, Phys. Rev. B **54**, 9353 (1996); Effect of interfaces on Gilbert damping and ferromagnetic resonance linewidth in magnetic multilayers, J. Appl. Phys. **90**, 4632 (2001).
[13] M. Tsoi, A. G. M. Jansen, J. Bass, W. C. Chiang, M. Seck, V. Tsoi, and P. Wyder, Excitation of a Magnetic Multilayer by an Electric Current, Phys. Rev. Lett. **80**, 4281 (1998); Erratum: Excitation of a Magnetic Multilayer by an Electric Current Phys. Rev. Lett. **80**, 4281 (1998); **81**, 493(E) (1998).
[14] J. A. Katine, F. J. Albert, R. A. Buhrman, E. B. Myers, and D. C. Ralph, Current-Driven Magnetization Reversal and Spin-Wave Excitations in Co/Cu/Co Pillars, Phys. Rev. Lett. **84**, 3149 (2000).
[15] I. M. Miron, K. Garello, G. Gaudin, P. J. Zermatten, M. V. Costache, S. Auffret, S. Bandiera, B. Rodmacq, A. Schuhl, and P. Gambardella, Perpendicular switching of a single ferromagnetic layer induced by in-plane current injection, Nature (London) **476**, 189 (2011).
[16] T. Suzuki, S. Fukami, N. Ishiwata, M. Yamanouchi, S. Ikeda, N. Kasai, and H. Ohno, Current-induced effective field in perpendicularly magnetized Ta/CoFeB/MgO wire, Appl. Phys. Lett. **98**, 142505 (2011).
[17] L. Liu, O. J. Lee, T. J. Gudmundsen, D. C. Ralph, and R. A. Buhrman, Current-Induced Switching of Perpendicularly Magnetized Magnetic Layers Using Spin Torque from the Spin Hall Effect, Phys. Rev. Lett. **109**, 096602 (2012).
[18] V. E. Demidov, S. Urazhdin, H. Ulrichs, V. Tiberkevich, A. Slavin, D. Baither, G. Schmitz, and S. O. Demokritov, Magnetic nano-oscillator driven by pure spin current, Nat. Mater. **11**, 1028 (2012).
[19] M. I. Dyakonov and V. I. Perel, Possibility of orienting electron spins with current, Sov. Phys. JETP Lett. **13**, 467 (1971).
[20] J. E. Hirsch, Spin Hall Effect, Phys. Rev. Lett. **83**, 1834 (1999).
[21] Y. A. Bychkov and E. I. Rashba, Oscillatory effects and the magnetic susceptibility of carriers in inversion layers, J. Phys. C **17**, 6039 (1984); G. Dresselhaus, Spin-orbit

coupling effects in zinc blende structures, Phys. Rev. **100**, 580 (1955).
[22] A. Manchon and S. Zhang, Theory of spin torque due to spin-orbit coupling, Phys. Rev. B **79**, 094422 (2009).
[23] U. H. Pi, K. W. Kim, J. Y. Bae, S. C. Lee, Y. J. Cho, K. S. Kim, and S. Seo, Tilting of the spin orientation induced by Rashba effect in ferromagnetic metal layer, Appl. Phys. Lett. **97**, 162507 (2010).
[24] W. G. Wang, M. Li, S. Hageman, and C. L. Chien, Electric-field-assisted switching in magnetic tunnel junctions, Nat. Mater. **11**, 64 (2012).
[25] L. Liu, C.-F. Pai, D. C. Ralph, and R. A. Buhrman, Magnetic Oscillations Driven by the Spin Hall Effect in 3-Terminal Magnetic Tunnel Junction Devices, Phys. Rev. Lett. **109**, 186602 (2012).
[26] R. H. Liu, W. L. Lim, and S. Urazhdin, Spectral Characteristics of the Microwave Emission by the Spin Hall Nano-Oscillator, Phys. Rev. Lett. **110**, 147601 (2013).
[27] H. Ulrichs, V. E. Demidov, S. O. Demokritov, W. L. Lim, J. Melander, N. Ebrahim-Zadeh, and S. Urazhdin, Optimization of Pt-based spin-Hall-effect spintronic devices, Appl. Phys. Lett. **102**, 132402 (2013).
[28] H. Ulrichs, V. E. Demidov, and S. O. Demokritov, Micromagnetic study of auto-oscillation modes in spin-Hall nano-oscillators, Appl. Phys. Lett. **104**, 042407 (2014).
[29] A. Slavin and V. Tiberkevich, Spin Wave Mode Excited by Spin-Polarized Current in a Magnetic Nanocontact is a Standing Self-Localized Wave Bullet, Phys. Rev. Lett. **95**, 237201 (2005).
[30] J. V. Kim, Q. Mistral, C. Chappert, V. S. Tiberkevich, and A. N. Slavin, Line Shape Distortion in a Nonlinear Auto-Oscillator Near Generation Threshold: Application to Spin-Torque Nano-Oscillators, Phys. Rev. Lett. **100**, 167201 (2008).
[31] A. Slavin and V. Tiberkevich, Excitation of spin waves by spin-polarized current in magnetic nano-structures, IEEE Trans. Magn. **44**, 1916 (2008); Nonlinear auto-oscillator theory of microwave generation by spin-polarized current, IEEE Trans. Magn. **45**, 1875 (2009).
[32] G. D. Fuchs, J. C. Sankey, V. S. Pribiag, L. Qian, P. M. Braganca, A. G. F. Garcia, E. M. Ryan, Z.-P. Li, O. Ozatay, D. C. Ralph, and R. A. Buhrman, Spin-torque ferromagnetic resonance measurements of damping in nanomagnets, Appl. Phys. Lett. **91**, 062507 (2007).
[33] S. Urazhdin, V. Tiberkevich, and A. Slavin, Parametric Excitation of a Magnetic Nanocontact by a Microwave Field, Phys. Rev. Lett. **105**, 237204 (2010).
[34] L. Xu and S. F. Zhang, Electric field control of interface magnetic anisotropy, J. Appl. Phys. **111**, 07C501 (2012).
[35] R. H. Liu, W. L. Lim, and S. Urazhdin, Control of current-induced spin-orbit effects in a ferromagnetic heterostructure by electric field, Phys. Rev. B **89**, 220409(R) (2014).
[36] X. Fan, H. Celik, J. Wu, C. Ni, K. J. Lee, V. O. Lorenz, and J. Q. Xiao, Quantifying interface and bulk contributions to spin-orbit torque in magnetic bilayers, Nat. Commun. **5**, 3042 (2014).